Theoretical and Applied Climatology (2025) 156:54
https://doi.org/10.1007/s00704-024-05247-4

RESEARCH

Climate characteristics and trends of extreme daily precipitation events associated with cold fronts in the metropolitan region of São Paulo, Brazil

Caroline Santos Segura[1] · Rosmeri Porfírio da Rocha[1] · Natália Machado Crespo[2]

Received: 5 July 2024 / Accepted: 10 November 2024 / Published online: 27 December 2024

Abstract
The metropolitan region of São Paulo (MRSP), located in southeastern Brazil, is densely populated and economically significant for the country. Cold fronts crossing MRSP are crucial for the precipitation regime and can induce extreme rainfall events. Therefore, this study presents a climatology of the contribution of cold fronts to extreme rainfall events in the MRSP and their associated synoptic patterns, using long term (1960 to 2022) local observations to identify cold fronts and daily rainfall extremes, and a time window of 5 days (from 2 days before and after). The mean circulation patterns associated with these events are analyzed using gridded precipitation and reanalysis for a short period (1980–2022). For 1960–2022, a total of 2535 cold fronts and 1077 extremes rainfall events were identified, with 58% of the daily extremes being associated with cold fronts. These events mainly occur during the austral spring, although their daily mean precipitation is higher in the austral summer. The contribution of cold fronts to extreme precipitation exhibits a statistically significant decrease, contrasting with the increasing trend in daily rainfall extremes. This suggests the influence of other meteorological systems in increasing rainfall extremes. The synoptic patterns reveal an intense anticyclone located southwest of the main trough in the lower troposphere, intense cyclonic vorticity along the front at low levels, stronger upper troposphere divergence, and strong thickness gradients in the 500–1000 hPa layer affecting MRSP. Most extremes occur on the day before and the day of the cold front due to more favorable dynamic conditions for convective activity.

1 Introduction

Analysis of past observations and future climate projections synthesized by the Intergovernmental Panel on Climate Change (IPCC) to provide their Assessment Reports (AR5, and AR6) have attracted attention to the more frequent and intense extreme weather events around the world (IPCC 2014, 2021). Many statistical indices may be used to characterize daily precipitation extremes, such as exceedance of a percentage of monthly/seasonal mean in one day (Carvalho et al. 2002; Liebmann et al. 2001) or the upper percentiles of daily rainfall (Carvalho et al. 2004; Sugahara et al. 2009; Silva Dias et al. 2013; Machado et al. 2021; Dalagnol et al. 2022; de Souza et al. 2024; Segura and da Rocha 2024). Moreover, the last International Panel on Climate Change (IPCC 2021) reports incorporated the use of percentiles to characterize extreme events to allow intercomparisons of the global extreme precipitation patterns and trends. The projections from the IPCC's sixth report indicate with high confidence that extreme precipitation events will become more frequent as global warming progresses. On a global scale, it is estimated that these events will intensify by 7% for each 1 °C increase in average global temperature (IPCC 2021). In continental regions, there is high confidence that the frequency and intensity of extreme precipitation have increased since 1950. The increase in extreme precipitation events is estimated to be caused by human-induced climate change. The threshold for defining a precipitation event as extreme varies depending on the location, climatological patterns (including synoptic systems) and seasonality of a specific region (Sugahara et al. 2009). Among the various

✉ Natália Machado Crespo
natalia.machado-crespo@matfyz.cuni.cz

[1] Departamento de Ciências Atmosféricas, Instituto de Astronomia, Geofísica e Ciências Atmosféricas, Universidade de São Paulo, Rua do Matão 1226, Cidade Universitária, São Paulo, SP, Brazil

[2] Department of Atmospheric Physics, Faculty of Mathematics and Physics, Charles University, V Holešovičkách 747/2, Prague 180 00, Czech Republic

meteorological systems that can produce extreme events are the cold fronts.

In South America, cold fronts significantly influence the weather conditions and climate year-round, moving preferentially from southwest to northeast. Cold fronts are synoptic-scale meteorological systems and are described as a boundary region between two air masses with different thermodynamic characteristics (Cavalcanti et al. 2009; Reboita et al. 2010; Reboita et al. 2023).

During austral winter, these systems often bring cold air masses from higher latitudes, causing cold spells and sometimes frosts in the south and southeast of Brazil as well as intense precipitation and winds (Garreaud 2000). In austral summer, cold fronts interact with warm and moist tropical air, leading to deep convection (Garreaud 2000; Nieto-Ferreira et al. 2011; Escobar et al. 2016). Considering the whole Southern Hemisphere, the climatology indicates cold fronts contributing to over 50% of the annual precipitation in mid-latitudes (Catto and Pfahl 2013).

The climatology of frontal systems conducted by Cavalcanti and Kousky (2003) in South America reveals a seasonal pattern, with a higher frequency of cold fronts during the winter and early-spring months (June to October), and a lower frequency between January and February (Escobar et al. 2019). There are two main paths for frontal systems over the continent: one inland, heading northwards from northern Argentina to the western Amazon region, and the other along the eastern coast of Brazil. More recent climatology of Pampuch and Ambrizzi (2015) found the north-central region of Argentina and southern Brazil experiencing between 45 and 50 cold front passages annually, while southeastern Brazil receives from 25 to 30 systems per year.

According to Seluchi et al. (2017), cold fronts responsible for intense rainfall in eastern Santa Catarina (Southern Brazil) are associated with the penetration of cold, intense, and weakly baroclinic troughs in the middle and upper levels of the atmosphere, as well as an intensification of a trough in the lower troposphere. Seluchi et al. (2016) also investigated the characteristics of cold fronts potentially responsible for intense rainfall events in the mountainous region of Rio de Janeiro (Southeastern Brazil); they showed that temperature contrast, vorticity advection, and upper-level divergence are important for the intensification of cold fronts. For the metropolitan region of Rio de Janeiro, Moura et al. (2013) found that fronts associated with intense rainfall in the area have three main modes (which explain 56% of the total variance of the cases). The first mode is characterized by fronts with zonal displacement; the second shows a pattern of fronts with intense post-frontal anticyclones; and the last mode indicates a pattern of post-frontal anticyclone to the east of Rio Grande do Sul, which results in southerly winds in Rio de Janeiro. In southern South America, Solari et al. (2022) showed that more intense cold fronts (stronger cyclonic vorticity and higher moisture content) are associated with extreme precipitation, and that dynamic factors play a crucial role for their occurrence.

Southeast Brazil is home of the largest metropolitan region in South America, São Paulo (MRSP), with a population of approximately 21.6 million in 2018 (IBGE 2018). This densely populated area is of great socio-economic importance for the country. In MRSP, cold fronts play a significant role in local weather patterns, particularly in terms of precipitation and temperature changes, being also important for pollutant dispersion. Observations in MRSP indicate several patterns associated with the passage of cold fronts. For example, the air temperature tends to rise in the day leading up to a front's passage followed by a decrease afterwards, while the wind typically shifts from northwest to south-southeast during and after the passage. In addition, cold fronts contribute substantially to seasonal precipitation, with austral winter and summer receiving approximately 59% and 41% of its precipitation from them, respectively (Dametto and da Rocha 2005; de Jesus 2014). In terms of frequency, cold fronts occur quasi-equally over the year, with a slightly greater occurrence in austral spring over the MRSP (Dametto e da Rocha 2005; de Jesus 2014). According to Escobar et al. (2019), almost 40% of the precipitation is associated with three baroclinic systems (cold fronts, subtropical fronts, and baroclinic troughs) during the rainy season, while this number increases to 60% during the dry season.

In MRSP, extreme precipitation events are more frequent from November to March, coinciding with the rainy season of southeast Brazil, when the highest volumes of precipitation occur (Liebmann et al. 2001; Carvalho et al. 2002; Sugahara et al. 2009). The extreme daily rainfall events are increasing in frequency and intensity in MRSP, leading to a statistically significant increase in total annual precipitation (Sugahara et al. 2009; Silva Dias et al. 2013; Marengo et al. 2020). Some studies related the increase in the occurrence of precipitation extremes with specific meteorological systems or changes in the urbanization in MRSP. For instance, Carvalho et al. (2004) linked the activity of the South Atlantic Convergence Zone to intraseasonal activity and the occurrence of extreme rainfall; Silva Dias et al. (2013) analyzed daily precipitation extremes using upper percentiles (80th, 95th, and 99th) to associate its increasing trends to the rapid urbanization and increasing pollutant concentrations; Vemado et al. (2016) studied severe weather episodes in the MRSP attributed to the combined effects of urban heat islands and sea breezes; Marengo et al. (2020) showed that the South Atlantic subtropical high underwent an intensification and a slight southwestward displacement from its normal position, which is modifies the moisture transport and could also explain the increase in extreme rainfall events in the MRSP. The substantial growth of rainfall extreme events in MRSP calls attention due to their impact on the region's

economy and human lives. Floods in MRSP are estimated to cause over 762 million Brazilian reais in damages annually (Haddad and Teixeira 2015).

Based on these findings, Marengo et al. (2020) concluded that the observed increase in annual rainfall totals in the MRSP is primarily a result of the rise in the frequency of extreme events. At the same time, a long-term analysis (1960–2022) does not indicate a statistically significant trend of the annual frequency of cold fronts in MRSP (Segura and da Rocha 2024). Therefore, despite the significant role of cold fronts in the precipitation climatology of MRSP, their contribution to extreme daily rainfall events as well as their change with the time in MRSP remains unclear.

In this context, this study aims to obtain a climatology and climate trends of the contribution of cold fronts to daily rainfall extremes events as well as to characterize the synoptic patterns associated with cold fronts producing extreme rainfall in the MRSP. Section 2 presents the data used and methods employed to identify the cold fronts and precipitation extremes; Section 3 shows the results on the daily and seasonal extremes associated with fronts and their spatial patterns; and Section 4 presents a summarization and conclusions.

2 Materials and methods

2.1 Data

In this study, three different datasets are employed. The first one comprises atmospheric variables (meridional wind, air temperature, and daily precipitation) from the meteorological station Paulo Marques dos Santos located at University of São Paulo Science and Technology Park at 799 m above sea level and in 23°39′S- 46°37′W. This station is used to represent MRSP and provides the data to identify cold fronts and their association with the daily precipitation extremes for the period 1960–2022.

The spatial patterns of rainfall associated with cold fronts in the MRSP are assessed through data from the Climate Hazards Group InfraRed Precipitation with Station Data (CHIRPS), which combines meteorological station observations and satellite-based precipitation estimates (Funk et al. 2015). CHIRPS was developed by the United States Geological Survey (USGS) and the Climate Hazards Group at the University of California, Santa Barbara (UCSB), and provides global daily precipitation analysis with a spatial resolution of 0.05º from 1981 to the present (Funk et al. 2015). Due to its high spatial and temporal resolutions, CHIRPS offers a novel alternative for studying precipitation extremes, which is particularly advantageous for climate studies, especially in regions with limited meteorological stations coverage.

ERA5 reanalysis provides the atmospheric data to obtain the spatial patterns related to extreme rainfall associated with cold fronts. ERA5 is the fifth generation of reanalysis produced by the Copernicus Climate Change Service at ECMWF and it replaces ERA-Interim (Hersbach et al. 2020). ERA5 has a horizontal resolution of 31 km and 137 vertical levels between the surface and 80 km-height covering the period from 1940 to the present. The refinement of resolution from ERA-Interim (80 km) to ERA5 (31 km) allows more detailed studies of synoptic-scale phenomena, showing more accurate features than ERA-Interim (Hersbach et al. 2020). From ERA5, 12 UTC data of geopotential and winds at different pressure levels, sea level pressure, and specific humidity at 850 hPa are used. From these data we derived the thickness layer between 1000 hPa and 500 hPa, relative vorticity, wind divergence and moisture flux.

2.2 Cold front identification

The objective method to identify cold fronts was previously employed by Jesus et al. (2016), Rodrigues and Sugahara (2004), Dametto and da Rocha (2005), and it has similarities with the method used by Pampuch and Ambrizzi (2015). The method consists in two conditions: (i) meridional wind component turning from the northern to the southern quadrant from day before (d-1) to the cold front day (d), remaining from the southern quadrant for at least 48 h after (d + 2) the turn; (ii) temperature drop either during the wind turning or within the following 48 h. This criterion for identifying fronts was validated by Segura and da Rocha (2024) by comparing with the records of cold front passages in southeast Brazil documented by Climanálise (a national publication that includes the dates and locations of the cold fronts crossing Brazil: http://climanalise.cptec.inpe.br/~rclimanl/boletim/). It was also verified by comparing with the three cases studied by Escobar et al. (2019): a classic cold front (12 July 2010 near São Paulo), which was correctly identified, and a subtropical front (19 May 2013 near Espírito Santo) and a baroclinic trough (5 March 2016 near MRSP), which were not identified as cold front by our criterion. Both verifications indicate the effectiveness of the used criterion in identifying cold fronts in the MRSP.

2.3 Detection of daily extreme rainfall

For the period 1960–2022, the 90th percentile of daily rainfall was calculated for each month, using only days with precipitation greater than zero of MRSP station data. The 90th percentile was chosen to provide a larger number of events with extreme daily rainfall to be associated with cold fronts. In addition, it is important to mention that there is a small difference between the 95th and 90th percentile precipitation thresholds. This approach is similar to that used by

Sugahara et al. (2009), who studied precipitation extremes based on upper percentiles. The percentile was calculated on a monthly basis because the definition of 'extreme precipitation' is dependent on seasonality, which provides different monthly amounts of rainfall to be considered an extreme event mainly in regions such as MRSP that presents a wet austral summer and dry austral winter (Sugahara et al. 2009).

2.4 Extreme rainfall events associated with cold fronts

The cold front algorithm provides a list of dates with cold front passages in the MRSP. From this information, daily precipitation data were filtered to select only days with cold front passage. By combining the dates of cold fronts and extreme events (above the 90th percentile), it was possible to select episodes of extreme daily rainfall occurring from two-day before (d-2) to two-day after (d + 2) the cold front passage. These events were thus divided into five groups: 'd-2', 'd-1', 'd', 'd + 1', and 'd + 2', each one representing the temporal interval in relation to the front's passage.

The characteristics of these events were compared with cold fronts without rainfall extremes (daily rainfall below the 90th), aiming to identify potential differences between the two scenarios. For example, 'd-2' group includes the daily rainfall extreme events (exceeding the 90th percentile) occurring two days before a cold front, which was then compared with 'd-2' cold fronts with daily rainfall below the 90th percentile. This allows studying the average and anomalous patterns of cold fronts associated with rainfall extremes for different atmospheric variables. It is important to note that the groups do not represent a temporal sequence; the events in the 'd-2' group are not necessarily connected to those in the 'd-1' group, and successively. They are different groups, involving events with potentially different characteristics.

It is important to emphasize that the requirement of a southerly wind for forty-eight hours limits the overlap of the same extreme event being included in more than one group. However, two events were identified that were associated with two different cold fronts. Therefore, each group contains unique events.

2.5 Time series analysis

Two statistical tests were employed for time series analysis: the Mann-Kendall test for monotonic trend detection (Mann 1945; Kendall 1975) and the Pettitt test for temporal series homogeneity (Pettitt 1979; Paiva and Sáfadi 2021). Both Mann-Kendall and Pettitt tests are non-parametric statistical tests described by Pohlert (2016). The Mann-Kendall test and Sen's slope test are two methods used to analyze trends in data over time.

The Mann-Kendall test is used to detect trends by comparing data points to each other over time. The analysis examines the direction of changes between successive points in the time series. The expression 'sign' refers to the sign (positive or negative) of the difference between pairs of points. When most differences are positive, it implies an upward trend; when the majority are negative, it indicates a downward trend (Segura and da Rocha 2024). The statistical test (S) is based on counting these changes (Pohlert 2016). On the other hand, Sen's slope is a way to calculate the magnitude of a trend in data over time. It compares all possible pairs of data points and calculates the slopes between them. Then, it finds the median of all these slopes, which represents the trend magnitude. This method is robust against outliers and works well for irregularly spaced data points. The Mann-Kendall test is calculated from the S statistic, shown in Eqs. 1 and 2 (Segura and da Rocha 2024).

$$S = \sum_{k=1}^{n-1} \sum_{j=k+1}^{n} sign(x_j - x_k) \tag{1}$$

$$sign(x) = \begin{cases} 1, & if\ x > 0 \\ 0, & if\ x = 0 \\ -1, & if\ x < 0 \end{cases} \tag{2}$$

$$U_t^+ = \sum_{j+1}^{t} \sum_{i=1}^{j} sign\left(x_j - x_i\right) \tag{3}$$

Equation 3 shows the variance of the S statistic, which in situations with very large samples assumes a normal distribution. N indicates the sample size (Segura and da Rocha 2024).

$$\sigma^2(S) = \frac{N(N-1)(2N+5)}{18} \tag{4}$$

Then, the Z-value is calculated to standardize the S statistic, as shown in Eq. 4.

$$Z = \begin{cases} \frac{S-1}{\sqrt{\sigma}}, & if\ S > 0 \\ 0, & if\ S = 0 \\ \frac{S+1}{\sqrt{\sigma}} & if\ S < 0 \end{cases} \tag{5}$$

The Pettitt test is calculated according to the U statistic, shown in the Eqs. (5), (6) and (7).

$$U = \left(U_t^+,\ U_t^-\right) \tag{6}$$

$$U_t^- = \sum_{j=t+1}^{n} \sum_{i=t+1}^{j} sign\left(x_j - x_i\right) \tag{7}$$

Here, 'x_i' represents the data value at time 'i', 't' is the potential change point, and 'n' is the total number of observations (Pohlert 2016). The change point is the time 't' that maximizes the test statistic U.

In essence, while the Mann-Kendall test identifies the presence of a trend in the data, Sen's slope test quantifies the magnitude of that trend (Pohlert 2016) and the Pettitt test identifies change points in the series. The significance level of 0.05 (p-value) is used to determine the statistical importance of potential trends and change points in the time series.

3 Results

3.1 Daily rainfall extremes

Table 1 presents the monthly values of the 90th percentiles of daily precipitation for the period 1960–2022 in MRSP. The 90th percentiles are higher in the austral summer (peaking in February) and lower in winter (lowest in August), following the annual cycle of precipitation (Fig. 1). For the thresholds in Table 1, a total of 1077 daily rainfall events exceeded the 90th percentile, resulting in an average of ~ 17 extreme events per year. As shown in Fig. 1, the seasonal variability of the mean frequency of the extremes follows the annual precipitation cycle: most events occurring in the rainy season (December to February; hereafter DJF), decreasing during the dry period (June to August; hereafter JJA).

The average monthly precipitation only considering extreme events is higher during the rainy season, reaching ~ 504 mm in January and 477 mm in February, highlighting these two months from the others of the year. July and August, which are typically the driest months, mean rainfall extremes only reach 98.4 mm and 76.8 mm, respectively.

Figure 2 presents the time series of absolute frequency of extremes and associated accumulated precipitation. There is a high interannual variability of the frequency of extreme rainfall events (above 90th percentiles), with some periods with less (e.g. 1960–1975) and more (e.g. 1977–1983 and near 2010) events (Fig. 2). The maximum number of events per year was 33 in 1976, and 2003 registered a minimum of 6 events. Figure 2 also makes evident that the interannual variability of the two series is remarkably similar, with an increase in the annual cumulative rainfall in the year with a higher number of extreme events and the opposite occurring when decreasing the number of extreme events, as previously documented for shorter time period (Sugahara et al. 2009; Silva Dias et al. 2013; Marengo et al. 2020).

Both series of accumulated extreme rainfall and annual frequency of extreme events indicate an increasing trend according to the Mann-Kendall test, with p-values of 0.013 and 0.025, respectively (Fig. 2). The slope of the trend is 0.07 for the frequency of annual events. Therefore, both the annual frequency of extreme events and the associated accumulated precipitation are increasing. The accumulated extreme precipitation is growing at a linear rate of approximately 4 mm per year. These results are in line with Sugahara et al. (2009), who found positive trends of the frequency

Table 1 Values of the 90th percentile of daily precipitation (mm day^{-1}) for each month calculated for the period 1960–2022 in MRSP

Month	Jan	Feb	Mar	Apr	May	Jun	Jul	Aug	Sep	Oct	Nov	Dec
90th	31.2	33.9	28.3	21.4	17.5	18.6	15.7	14.7	19.1	24.1	25.4	27.6

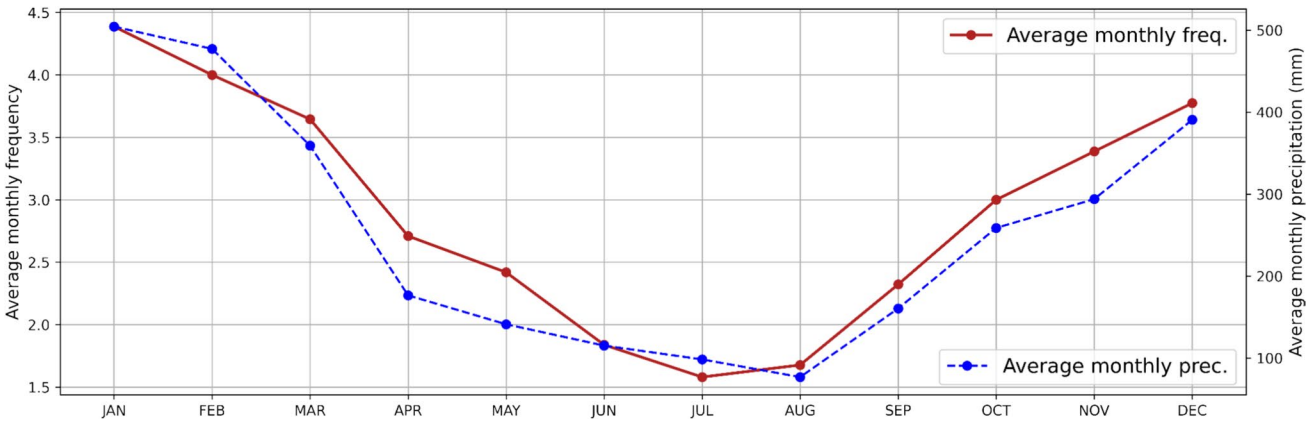

Fig. 1 Annual cycle of the mean frequency of extreme rainfall events (counts, left scale) and associated average monthly mean extreme precipitation (mm, right scale) for the period 1960–2022 in the MRSP

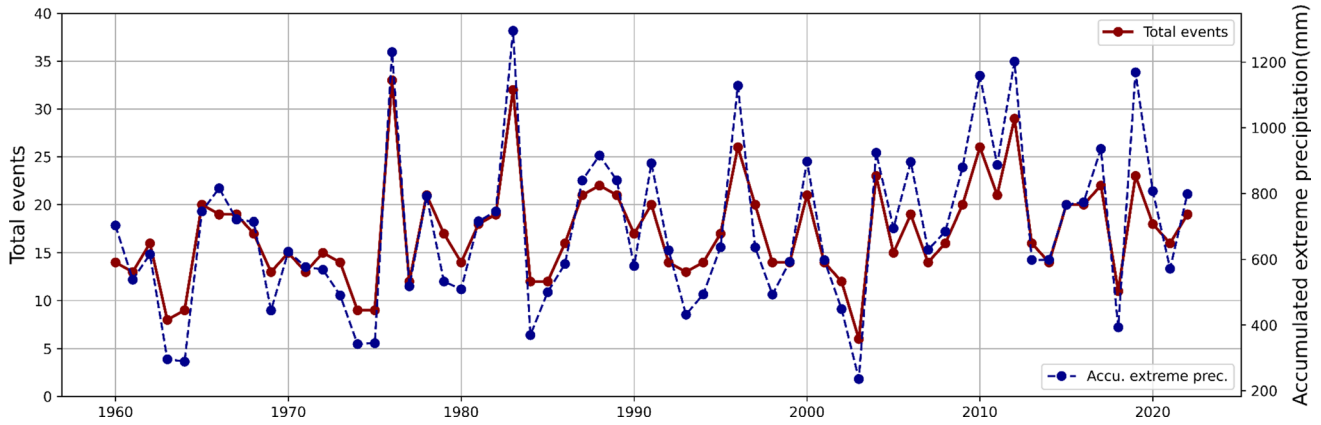

Fig. 2 Time series of extreme rainfall events (absolute number, left scale, red line) and associated accumulated precipitation (mm, right scale, dashed blue line) for the period 1960–2022 in the MRSP

and intensity of rainfall extreme events in the MRSP station time series for the period 1933–2005.

3.2 Annual and seasonal rainfall extremes associated with cold fronts

Using the objective criterion (Section 2.2), 2534 cold fronts were identified from 1960 to 2022. This gives an average frequency of approximately 40 cold fronts per year crossing the MRSP, with a minimum of 32 (in 1998) and a maximum of 50 (in 2009).

Figure 3 shows the boxplot for the annual cycle of cold fronts in the MRSP, which gives a more detailed understanding of the seasonal variations in cold front passages through the region. It is noted that during September to November (SON) the frequency of cold fronts is higher, with a median of four fronts in September and October and outliers reaching a maximum of seven and a minimum of two systems. For January and February, the variability is similar to that of June, which has a minimum number of fronts. However, in January and February there is a higher occurrence of outliers, up to six and seven fronts, respectively. The greater interquartile range of cold fronts frequency occurs in July and November.

As described in Section 2.4, the association between daily precipitation extremes and cold fronts considered a time window of 5 days (from two days before to two days after). This time window is based on the analysis characterizing cold fronts in southern Brazil (Rodrigues and Sugahara 2004). Applying a 5-day window, from 1077 extreme events, 630 of them are related to the passage of cold fronts, which indicates that 58% of the cold fronts produce daily rainfall extremes in MRSP.

This percentage is moderately higher than obtained by Lima et al. (2010), who associated the cold fronts with ~ 53% of extreme daily rainfall events in southeastern Brazil. However, it is in the range of the one obtained by Catto and Pfahl (2013) in mid-latitudes in the Southern

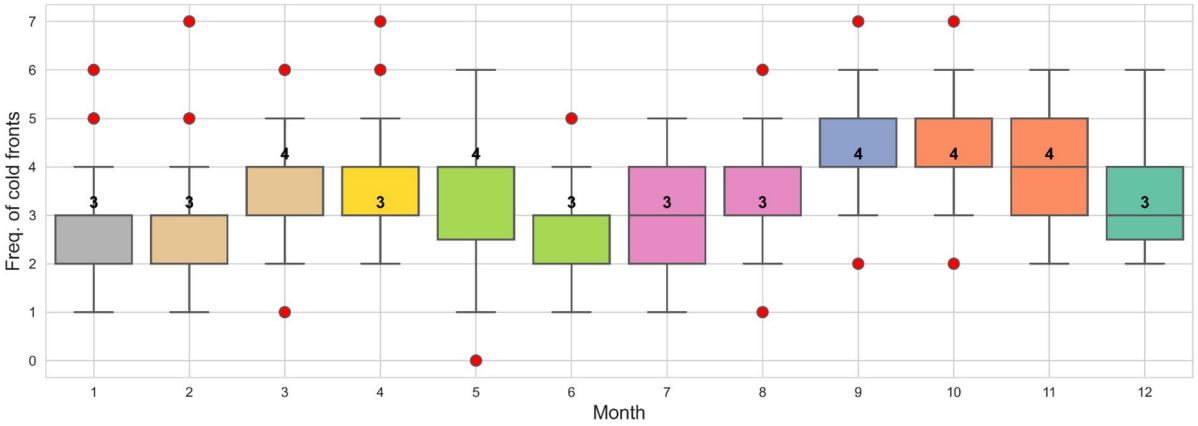

Fig. 3 Boxplot for the annual cycle of all cold fronts in the MRSP during 1960–2022. For each month, the boxplot displays the outliers, minimum value, first quartile, median (numbers in the boxes), third quartile, and maximum value for the frequency of cold fronts

Hemisphere, where cold fronts contribute to over 50% of the total precipitation.

The higher number of extreme events associated with fronts (209) occur one day before the cold front ('d-1'), which is explained by the synoptic environment analysis (Section 3.5). The day of the fronts ('d') has 173 extremes and for both ('d-1' and 'd') the average extreme precipitation reaches 39.3 mm/day. However, although less frequent, the events occurring two days before the cold front are slightly more intense, with average daily extreme precipitation of 41.6 mm/day. The average daily precipitation, considering all cold fronts and not just extremes, is much lower than for cold fronts associated with extremes (Table 2).

For cold fronts with extreme events, the highest average daily rainfall occurs on 'd-2' (41.6 mm/day), while this occurs in 'd-1' for cold fronts without extremes (6.4 mm/day). Table 2 also presents an increase in the average precipitation between 'd + 1' and 'd + 2' for both cold fronts with and without extreme rainfall.

Table 3 displays the seasonal absolute frequency and mean extreme precipitation of cold fronts crossing MRSP (from 'd-2' up to 'd + 2'). SON has a greater frequency of days with cold fronts associated with rainfall extremes, being also the season with the highest frequency of cold fronts (Dametto and da Rocha 2005; de Jesus 2014; Segura and da Rocha 2024), followed by MAM and DJF. The lowest frequency occurs in JJA. In all seasons, the rainfall extremes associated with fronts are more frequent in 'd-1' and 'd' and less frequent in 'd + 1' in DJF, SON and MAM (Table 3). It is interesting to note that even though the highest frequency of events occurs in SON, the highest average precipitation is registered in DJF, coinciding with higher precipitation climatology in the region. A possible explanation for the greater intensity of events in DJF is the occurrence of low-level jet episodes. During the austral summer, the moisture flow from the Amazon is intensified, creating a more favorable environment for heavier rainfall episodes (Montini et al. 2019). Another possible mechanism capable of explaining the higher intensity of events in DJFter is the increased frequency of episodes of the South Atlantic Convergence Zone (SACZ), which is more common in austral summer (Silva et al. 2021). The higher frequency of extreme precipitation events in SON can be explained by the return of the rainy season in southeastern Brazil, which is associated with increased available moisture and a higher frequency of fronts favoring the occurrence of intense rainfall events.

Figure 4 shows a boxplot of the seasonal variation in precipitation associated with extreme rainfall events due

Table 2 Number of extreme rainfall events and daily mean precipitation (mm/day) for cold fronts with and without daily rainfall extremes from two days before (d-2) until two days after (d + 2) the cold fronts in the MRSP for the period 1960–2022

Time	d-2	d-1	d	d + 1	d + 2
Number of extreme events	89	209	173	69	90
Annual mean extreme events	1.4	3.4	2.8	1.1	1.5
Average *daily extreme precipitation* associated with cold fronts	41.6	39.3	39.3	35.3	36.2
Average daily precipitation for all cold fronts	3.8	6.4	5.6	2.8	3.0
Extreme rainfall anomaly associated with cold fronts	37.8	32.9	33.7	32.5	33.2

Table 3 Seasonal absolute frequency (absolute number) of rainfall extreme associated with cold fronts and corresponding mean precipitation (mm/day), and the total number of cold fronts in the MRSP for the period 1960–2022

Time	DJF (freq)	DJF Mean rainfall (mm/day)	MAM (freq)	MAM Mean rainfall (mm/day)	JJA (freq)	JJA Mean rainfall (mm/day)	SON (freq)	SON Mean rainfall (mm/day)
d-2	27	**47.7**	24	38.6	6	37.8	**32**	39.4
d-1	56	**48.3**	57	37.3	27	32.2	**69**	36.5
d	50	**50.4**	39	37.2	33	26.6	**51**	38.1
d + 1	14	**45.4**	**23**	38.4	18	26.5	14	31.5
d + 2	20	**49.0**	27	36.8	12	31.5	**31**	34.6
Total of days of cold fronts with rainfall extremes	167		170		96		**197**	
Seasonal mean	2.7	**48.2**	2.7	37.6	1.5	30.9	3.2	36.0
Total of cold fronts	568	-	646		551	-	**769**	

Bold indicates the maximum for each season

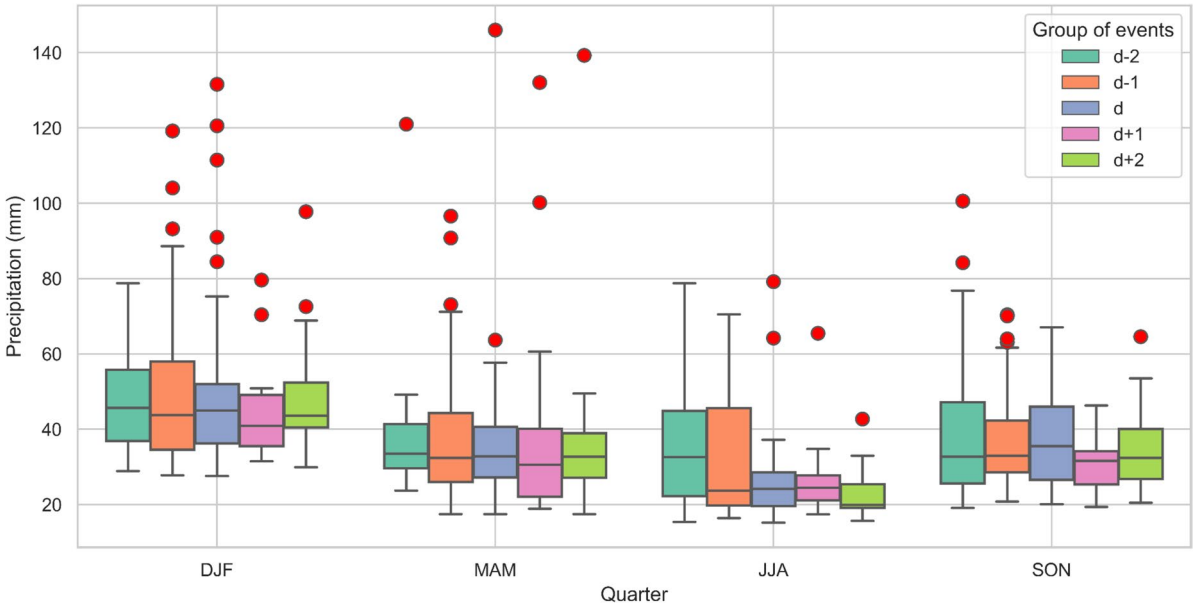

Fig. 4 Boxplot for the annual cycle of extreme daily precipitation (mm/day) associated with cold fronts for each group of events: 'd-2' (green), 'd-1' (orange), 'd'(blue), 'd + 1' (pink), 'd + 2' (olive green)

to the passage of cold fronts over the MRSP. It is notable that DJF has the larger number of outliers, with rainfall above 80 mm/day (10 events), and with half of these outliers recorded on the day of the cold front passage. Three outliers are recorded in the 'd-1' group (one day before the passage). March to May (MAM) is the only season showing outlier events with rainfall equal to or above 140 mm per day (2 events). One of these events was recorded in the 'd' group, and the other in the 'd + 2' group. For JJA, the events show a lower amount of precipitation compared to the wetter period. However, there are still records of intense daily rainfall events, between 40 and 80 mm/day. The 'd' group registers two outlier events with daily rainfall between 60 and 80 mm/day. In SON there are 5 outliers, two of which occur in the 'd-2' group, and these are also the events with the highest daily rainfall from 80 mm/day to 100 mm/day. Two events occuring in the 'd-1' have daily rainfall between 60 and 80 mm/day, and the single outlier in the 'd + 2' accumulates over 60 mm/day.

It is interesting to note that during JJA (the dry season in southeastern Brazil) the maximum values for the 'd-2' and 'd-1' groups are comparable to the maximum values for the same groups during the rainy season. Overall, the minimum rainfall values for all groups in JJA are also comparable and not substantially different from the minimum in MAM and SON. However, the rainfall maximum for 'd', 'd + 1' and 'd + 2' are lower in JJA (though still close to 40 mm/day).

3.3 Trends of extreme rainfall associated with cold fronts

The time series of extreme rainfall events associated with cold fronts over the MRSP was constructed considering the sum of events occurring from 'd-2' to 'd + 2'. Figure 5a (red line) shows an average of 10 events per year, ranging from ~ 3 (in 1985 and 2003) to 20 (in 1983), followed by 1976 with 19 events. This series does not show a monotonic trend or regime change points according to Mann-Kendall and Pettitt tests, respectively.

The accumulated extreme precipitation associated with cold fronts is presented in Fig. 5a (blue line). For the whole period, the average rainfall reaches 388.7 mm/year, with 1983 and 2019 standing out with accumulations of 755.0 and 749.2 mm/year, respectively, which are the highest amounts in the series representing 300 mm above the average. The accumulated extreme rainfall associated with fronts for 1983 represents 194.2% of the average and 2019 represents 192.7% of the average. The years 1985 and 2003 have the lowest accumulations of extreme rainfall associated with cold fronts, with 90.2 and 105.8 mm/year, respectively. The series also does not show a monotonic trend (p-value equal to 0.81) or regime change points.

The relative contribution of extreme rainfall associated with cold fronts to the total rainfall for all extreme days is shown in Fig. 5b. On average, more than half (57.4%, Fig. 5b) of the extreme precipitation accumulation is associated with cold fronts in the MRSP. According to Fig. 5b,

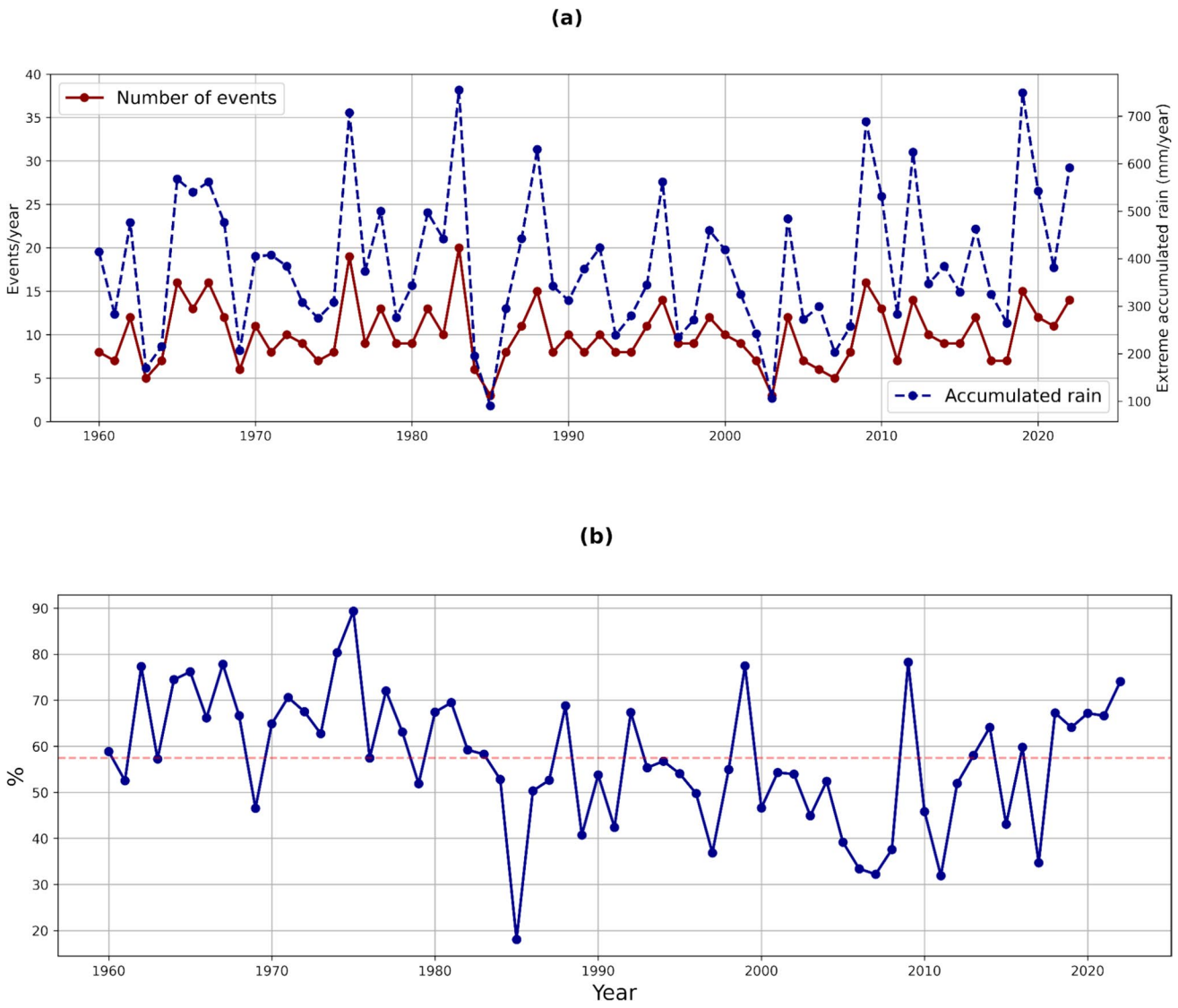

Fig. 5 **a** Annual mean absolute frequency of extreme precipitation events associated with cold fronts (events/year, red line) and accumulated rainfall (mm/year, blue line) in the MRSP. **b** Relative contribution (%) of extreme rainfall associated with cold fronts to the total rainfall for all extreme days. Dashed line indicates the average

some years stand out with higher relative contributions, such as 1975, 1974, 2009, and 1999 representing 89.3%, 80.4%, 78.2%, and 77.4%, respectively. It is interesting to note that the higher contribution in 1975 and 1974 resulted from between 7 and 8 extreme rainfall events, while 16 occurred in 2009. The lowest relative contributions of cold fronts to extreme rainfall occurred in 1985, 2011, 2007 and 2006, with 18.0%, 31.8%, 32.2% and 33.4%, respectively (Fig. 5b).

Figure 5b presents a statistically significant monotonic decreasing trend (p-value equal to 0.051) and a regime change point in 1984 (p-value equal to 0.0007). The relative contribution of cold fronts to extremes before and after the change point are 66.2% and 52.1%, respectively. It is noticeable from 1960 to 1984 that most years remain above the average, while the opposite (years below the average) occurs afterwards (1985–2022; Fig. 5b).

The negative trend observed in Fig. 5b, when compared with Fig. 2, and 5a, indicates that extreme rainfall associated with cold fronts does not show a decreasing trend. However, the contribution of cold fronts to extreme precipitation exhibits a statistically significant decrease. Such a trend may suggest an increase in daily rainfall extremes due to other forcings, such as rainfall organized by sea breeze (Perez and Silva Dias 2017), isolated convection forced by urbanization effect (Vemado and Pereira Filho 2016), or changes in subtropical anticyclones over the South Atlantic with consequent increase of moisture transport to the region feeding the intense convection (Marengo et al. 2020).

3.4 Spatial pattern of extreme rainfall associated with cold fronts

As CHIRPS data is available only after 1981, the composites were calculated considering only cold fronts in the MRSP for the period 1981–2022. Figure 6 displays CHIRPS spatial pattern of precipitation anomaly for the five days (from 'd-2' until 'd + 2') used to analyze the cold fronts. The anomalies were calculated as the difference between the composites for the cold fronts with and without daily rainfall extremes.

According to the CHIRPS database, the most intense positive anomalies are observed on the day of the cold front, with up to 15 mm/day concentrated in the MRSP and coastal areas (Fig. 6c). Extreme events occurring on 'd-1' exhibit a pattern with positive rainfall anomalies in southern Minas Gerais and northeastern state of São Paulo (up to 9 mm/day) and negative ones to the south of the state. For the 'd-2', the positive anomalies are more confined to the neighborhood of MRSP, and with lower intensity (up to 4 mm/day) than for 'd' and 'd-1'. On 'd + 1' and 'd + 2' the more intense positive anomalies occupy the coastal area of the state of São Paulo, still encompassing the southern portion of MRSP (Fig. 6d, e).

Although CHIRPS captures the spatial pattern of anomaly of precipitation for extreme events associated with cold fronts, the differences in intensity between CHIRPS (Fig. 6) and MRSP station (Table 2) are high. This is expected because MRSP station represents only one grid point, which may be subject to large local variations not captured by CHIRPS gridded data. The processes of interpolation and use of multiple sources of data (local observations, satellite estimates, reanalysis, etc.) in general reduces the ability of gridded analysis to capture extreme rainfall, as discussed also by Cavalcante et al. (2020) when analyzing the Amazon sector of South America.

Table 4 shows the average daily rainfall for MRSP location considering all event groups, according to the CHIRPS database. Overall, there is an apparent underestimation of the rainfall totals from the events according to the CHIRPS

Table 4 Average daily rainfall (mm/day) for 'd-2' to 'd + 2' at MRSP location (average in a 1.0° x 1.0° box centered on the IAG-USP station) according to the CHIRPS database for the period 1981–2022

Event	d-2	d-1	d	d + 1	d + 2
Mean rainfall CHIRPS (mm day^{-1})	11.6	14.6	20.7	12.7	9.3

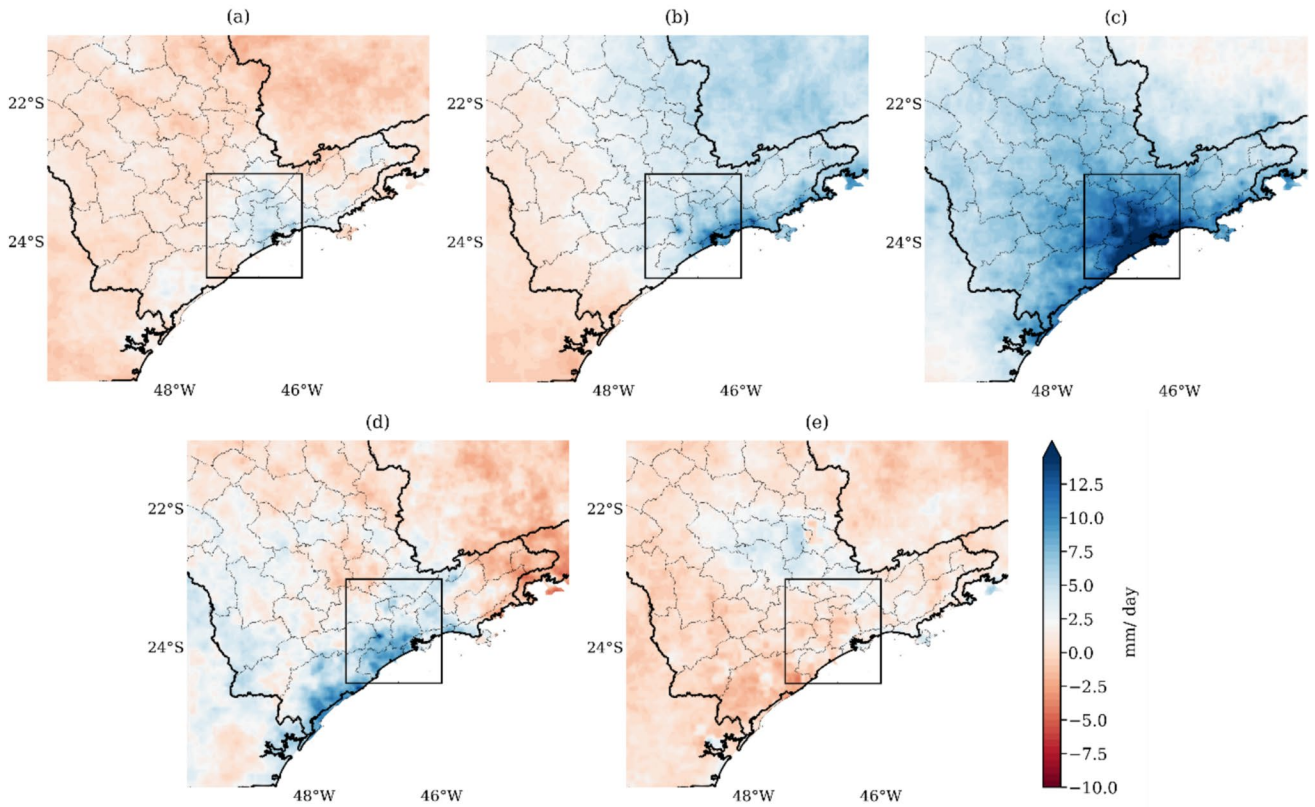

Fig. 6 CHIRPS daily precipitation averages anomaly for extreme precipitation (mm/day) associated with the cold fronts in the MRSP: **a** 'd-2', **b** 'd-1', **c** 'd', **d** 'd + 1', **e** 'd + 2'. The square highlights a large area around MRSP

data. The highest average occurs in the 'd' group, with only 20.7 mm/day (~50% less precipitation), showing values that are significantly different from those presented in Table 2. The largest difference occurs in the 'd + 2' group, with a 27.6 mm difference between the average obtained from CHIRPS and the average from IAG (around 75% less precipitation).

Table 5 shows the 90th percentiles for CHIRPS database; it is noticeable that CHIRPS presents small differences when compared to the 90th percentile calculated using precipitation from MRSP (or IAG station) shown in Table 1. For January and February, for instance CHIRPS are slightly higher, while in the remaining months they are lower, with the largest difference occurring in April.

3.5 Synoptic features of extreme rainfall associated with cold fronts

The composites of atmospheric fields are presented for the same period of CHIRPS data, i.e., 1981–2022. For this period, the anomalies were calculated as the difference between cases of cold fronts associated with extreme rainfall events and of cold fronts not associated with extreme rainfall events.

Figure 7 depicts the composites of the wind at 1000 hPa and sea-level pressure for cold fronts associated with rainfall extremes. It is noted that São Paulo is under the influence of a relative low-pressure area, with the associated surface cyclone (in this case, a cyclone is the same as a low-pressure area) located over the South Atlantic Ocean (40°W; 50ºS) far from the MRSP. Southwestward and away of the MRSP (over southern Brazil, Uruguay and northeastern Argentina) there is a post-frontal anticyclone sustaining south/southeasterly winds to the MRSP, while the South Atlantic subtropical anticyclone (SASA) is displaced to the east contributing to intensify northerly winds. These winds are prevalent from 'd-2' to 'd + 2' and favor the transport of moist air from the ocean to the continent, which strengthens the hypothesis that moisture from the ocean is a crucial factor to trigger extreme rainfall events in MRSP (Marengo et al. 2020).

In Fig. 7, for 'd-2' to 'd + 2' groups, the cold front at the surface is located near the northern part of the state of São Paulo, in the vicinity of the Rio de Janeiro coast. The lack of variation in the surface front's position across the groups might be related to the fact that the analysis does not consider the same cold front sequentially over time. However, the analysis of meridional wind for the event groups using MRSP data reveals that for the 'd-2' and 'd-1' groups, there is a prevalence of northwesterly winds, which is consistent with a pre-frontal situation. In this case, there might be some discrepancies between the synoptic environment shown by the ERA5 reanalysis and the environment suggested by the MRSP data meteorological station.

Magalhães et al. (2023) also emphasizes that cold fronts causing more intense winds are associated with the presence of amplified trough reaching the northern part of the Santos Basin, which is similar to the day 'd' (Fig. 7c), where the frontal trough is quite close to the coast of the state of São Paulo. Thus, it is plausible that the structures and characteristics presented by Magalhães et al. (2023) are also related to events of heavy rainfall.

Investigations conducted by Andrade and Cavalcanti (2018) showed that frontal systems associated with intense rainfall are related to a low-pressure system acting near the east of South America, which differs from this study, where the low pressure is southeastward away from the region (Fig. 7). However, similar to Andrade and Cavalcanti (2018), cold fronts associated with extreme rainfall also have a strong post-frontal high-pressure system (Fig. 7).

Bonnet et al. (2018) noted that for the cases of post-frontal rainfall events in Rio de Janeiro, both the trough and the post-frontal anticyclone have a more amplified structure than cold fronts without post-frontal rainfall. Moura et al. (2013) also emphasized the significance of the post-frontal anticyclone for the occurrence of extreme precipitation in Rio de Janeiro. They demonstrated that on the day of the extreme rainfall, the post-frontal anticyclone intensifies the pressure gradient between oceanic and continental regions, resulting in winds from the south transporting moist air from the ocean to the continent. These patterns resemble the 'd + 1' and 'd + 2' composites in Fig. 7.

Figure 8 depicts composites of the geopotential height at 500 hPa and anomalies of thickness between 500 and 1000 hPa. From 'd-2' to 'd + 2' (Fig. 8), the geopotential height at 500 hPa characterizes a trough near MRSP, with an axis northwest-southeast oriented extending over the South Atlantic Ocean. As indicated by the negative thickness anomaly, this system is especially intense (cold) on 'd-1' when the number of rainfall extremes associated with cold fronts is highest (Table 2). On day 'd' (Fig. 8c), the negative thickness anomaly is over a smaller portion of the continent, southern 20ºS, much less intense than in 'd-1'.

Table 5 Values of the 90th percentile of daily precipitation (mm day^{-1}) for each month calculated for the period 1981–2022 at MRSP location (average in a 1.0° x 1.0° box centered on the IAG-USP station) according to the CHIRPS database

Month	Jan	Feb	Mar	Apr	May	Jun	Jul	Aug	Sep	Oct	Nov	Dec
90th	29.9	29.3	31.8	28.2	24.3	21.5	16,0.6	16.9	25.8	29.2	26.2	27.5

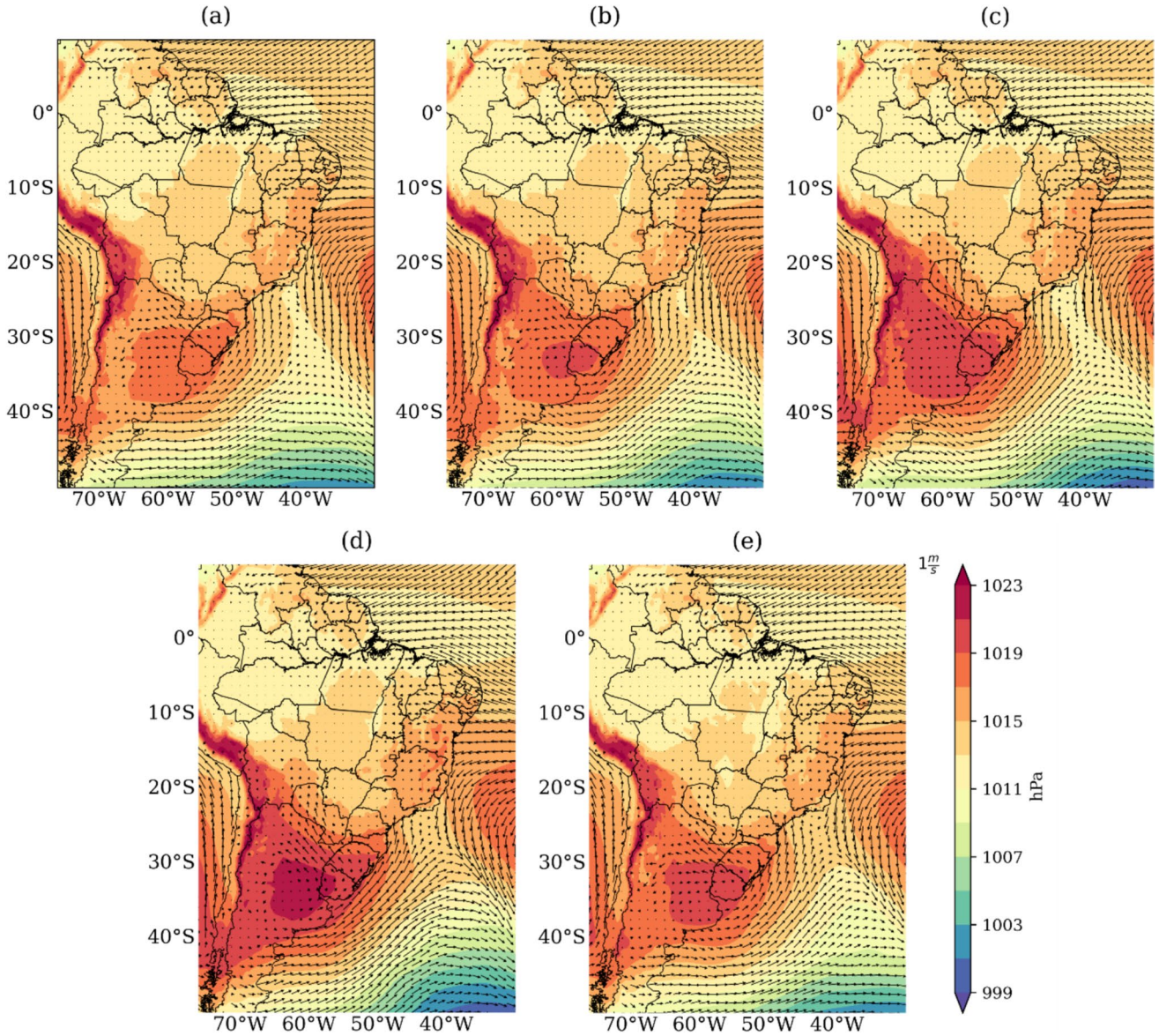

Fig. 7 Composite fields of sea level pressure (shaded, hPa) and wind at 1000 hPa (m/s) for extreme rainfall events associated with cold fronts in MRSP for: **a** 'd-2', **b** 'd-1', **c** 'd', **d** 'd + 1', **e** 'd + 2'. Composites are calculated from ERA5 reanalysis for the period 1981–2022

The thickness anomalies in Fig. 8 indicate that cold fronts associated with extreme rainfall events exhibit a stronger temperature gradient (due to the greater thickness gradient in the layer 500–1000 hPa), with a consequently likely greater vertical wind shear, stronger upper-level jet streak (Martin 2013). This configuration provides stronger dynamic support for the extreme events.

Composites of streamlines and wind divergence anomaly at 250 hPa are shown in Fig. 9. A prominent and dominant pattern in streamlines is an upper-level circulation resembling those of austral summer months, with an anticyclonic circulation in the northwest of the continent, and a trough structure downstream located in northeastern Brazil (Fig. 9a-e). This pattern is consistent with the structure of the Bolivian High displaced to the northwest compared to climatology and it was also found by Seluchi et al. (2016) when analyzing cold fronts. The location of the Bolivian High's circulation further north may provide a more favorable environment for frontal systems to penetrate the continent. Andrade and Cavalcanti (2018) also studied patterns of cold fronts associated with heavy rainfall, showing that in cases of non-rainy fronts, the typical pattern of the Bolivian High is displaced southward over the continent, which would hinder the continental advancement of the fronts.

The westerly circulation occupying the latitudinal band 20–30°S at upper levels (250 hPa), between the trough in

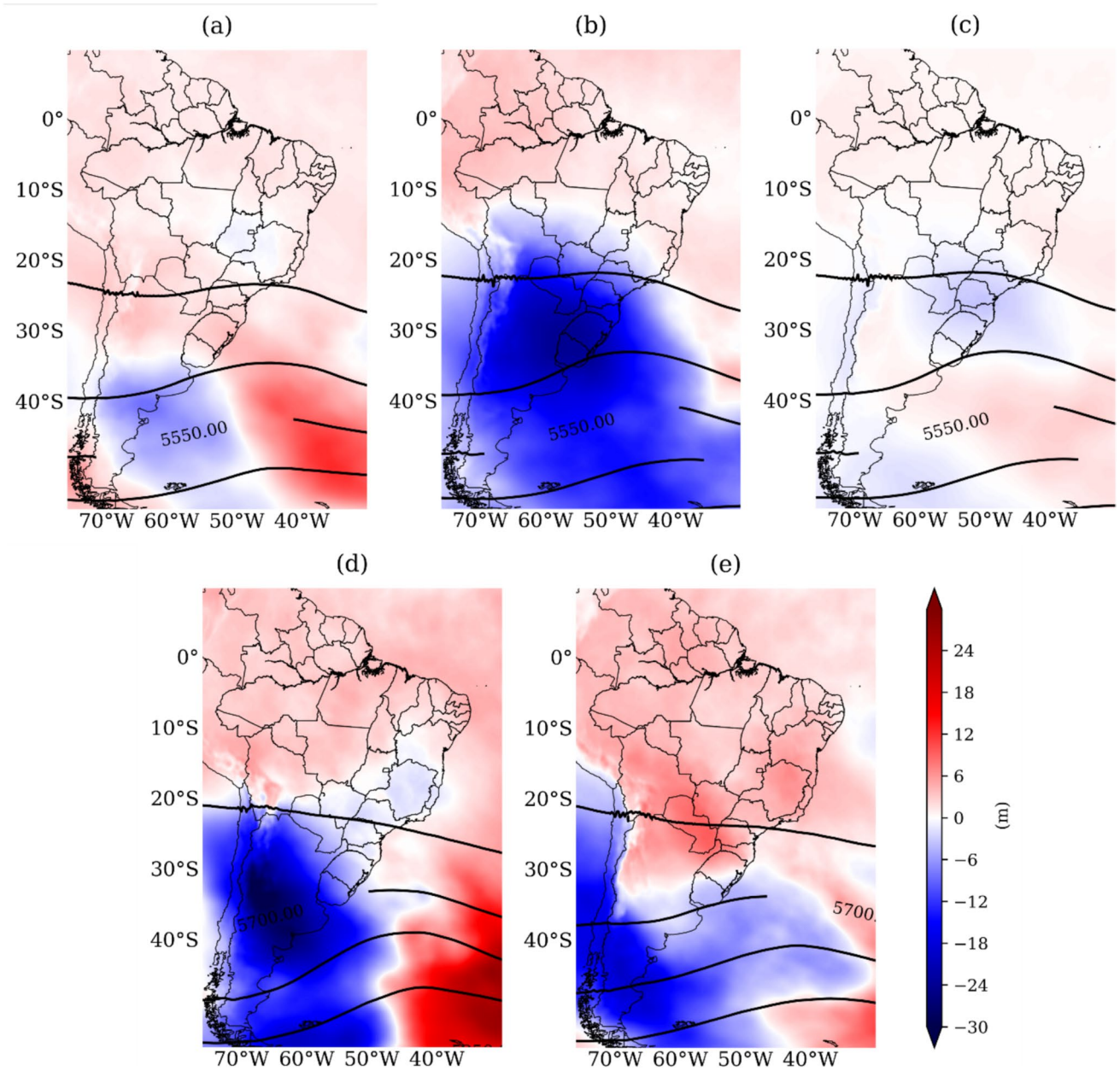

Fig. 8 Mean geopotential height at 500 hPa (solid lines, in meters) and thickness anomaly between 500–1000 hPa (shaded, in meters) for extreme rainfall events associated with the cold fronts in MRSP for: **a** 'd-2', **b** 'd-1', **c** 'd', **d** 'd + 1', **e** 'd + 2'. Composites are calculated from ERA5 reanalysis for the period 1981–2022

southern South America and the one in northeastern Brazil, creates conditions for intensifying the mass divergence, which contribute to intensifying convective activity over center-southeast Brazil. This divergence is stronger over São Paulo on days 'd-1', 'd' and 'd + 1' compared with 'd-2' and 'd + 2' (Fig. 9). The upper-level westerly circulation (axis in ~ 25°S) with associated anomalous wind divergence acts to intensify the convective activity over MRSP and surroundings. It is interesting to note that the 'd-1', 'd' and 'd + 1' groups exhibit higher values of divergence occupying larger areas at upper levels, which possibly indicates greater dynamic support for the occurrence of extreme rainfall events. This is in line with the study of the development and strengthening of the summer thunderstorms in the MRSP conducted by Rodriguez et al. (2010), which found wind divergence anomalies at 250 hPa similarly as in Fig. 9.

Comparing Figs. 8 and 9, on all days the trough located in the southern of the South Atlantic Ocean presents a relatively low slope between the 500 hPa and 250 hPa levels. This weak vertical inclination was also observed by Seluchi

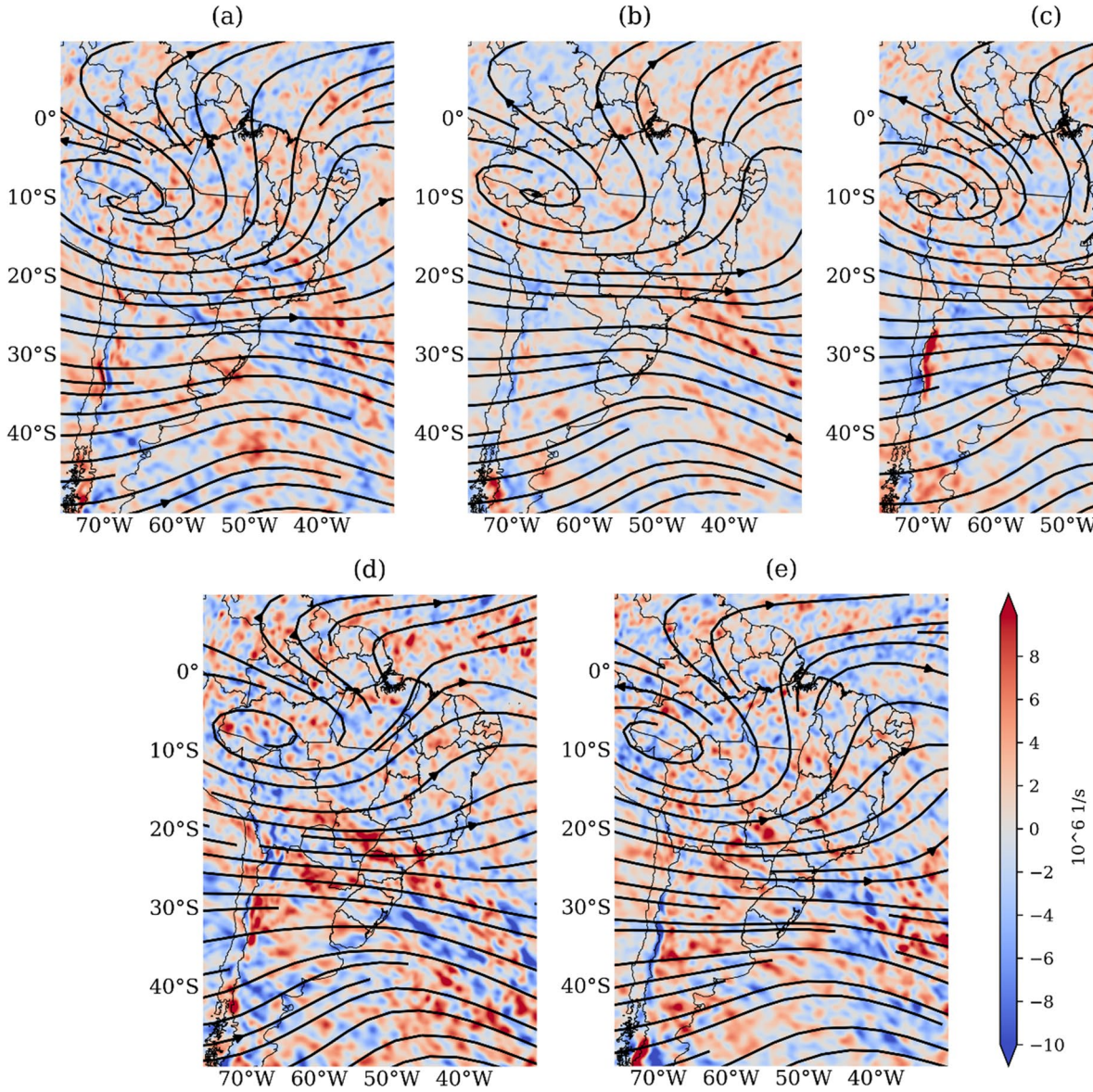

Fig. 9 Composites of streamlines and anomaly of wind divergence (shaded; in units of 10^{-6} s^{-1}) at 250 hPa and for each group of extreme rainfall events associated with the cold fronts in MRSP for: **a** 'd-2', **b** 'd-1', **c** 'd', **d** 'd+1', **e** 'd+2.' Composites calculated from ERA5 reanalysis for the period 1981–2022

et al. (2017) in a study characterizing the cold fronts causing intense rainfall in Santa Catarina (south Brazil).

From 'd-2' to 'd+2', the cold fronts associated with rainfall extremes are characterized by the presence of a frontal trough and anomalous intense northwest-southeast organized band of cyclonic vorticity at 850 hPa crossing center-western São Paulo state, which is more continental and organized from 'd-1' to 'd' (Fig. 10). The low-level circulation further shows the confluence over MRSP of the northwesterly flow with origin in Amazon basin with northerly winds from western side of SASA. The presence of an extratropical anticyclone over Argentina inducing southeasterly flow over part of southern Brazil is also well characterized from day 'd-2' to 'd+2'.

From Figs. 7 and 10, it is noted that the circulation at 1000 hPa is predominantly from the south/southeast, however, at the 850 hPa level there is the presence of northwesterly winds. This indicates a more inclined frontal ramp between 1000 − 850 hPa, as also noted by Seluchi et al. (2017).

Figure 11 shows the moisture flux anomaly (vectors and intensity). From 'd-2' to 'd+2', there are positive anomalies of moisture flux over the Southern and Southeastern regions of Brazil for cold fronts associated with extreme rainfall. For the 'd-2' (Fig. 11a) the positive anomalies of moisture

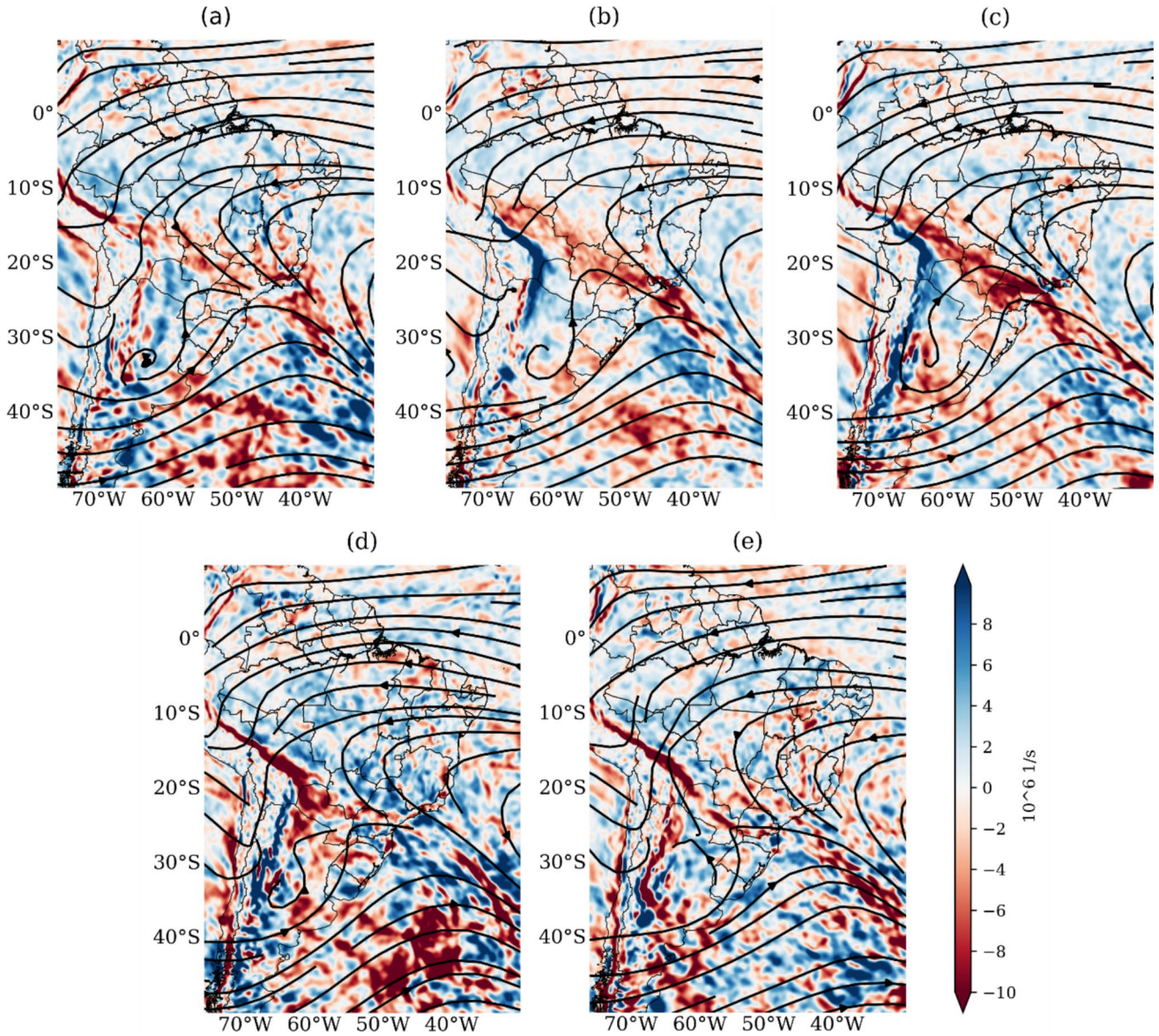

Fig. 10 . Composites of vorticity anomaly ($x10^{-5}s^{-1}$) and mean streamlines at 850 hPa for extreme rainfall events associated with the cold fronts in MRSP for: **a** 'd-2', **b** 'd-1', **c** 'd', **d** 'd + 1', **e** 'd + 2'. Composites are calculated from ERA5 reanalysis for the period 1981–2022

flux are located especially northward of MRSP, which turns cyclonically near the coast of the state of São Paulo (centered at approximately 27°S; 40°W), with south/southeasterly being responsible to moisture flux to the MRSP.

In the 'd-1' and 'd' (Fig. 11b, c), positive anomalies associated with anomalous cyclonic circulation are enhanced (centered approximately over eastern MRSP), consequently intensifying the northwesterly winds circulation and allowing southeasterly flow, both acting to increase the moisture flux, especially in the proximity of MRSP. High positive moisture flux anomalies also occur in 'd-1' over Rio de Janeiro, parts of Minas Gerais and Goias states as well as on day 'd' over a great part of São Paulo and other states (Rio de Janeiro, Minas Gerais, southern Goiás and Mato Grosso do Sul). Positive anomalies of southerly moisture flux over the region of Bolivia are also intensified in day 'd'. For 'd + 1' and' d + 2' (Fig. 11d, e), there is an intense northwesterly moisture flux from Amazon to the south/southeast of Brazil, more intense on 'd + 1'.

Most events are concentrated between one day before ('d-1') and on the day of the front ('d'). These days stand out in the composites, especially due to cyclonic vorticity anomalies along the front line. The anomalies are more pronounced and appear to be better organized from Bolivia to the South Atlantic Ocean adjacent to the eastern coast of southeastern Brazil, with the frontal system visibly more extensive and

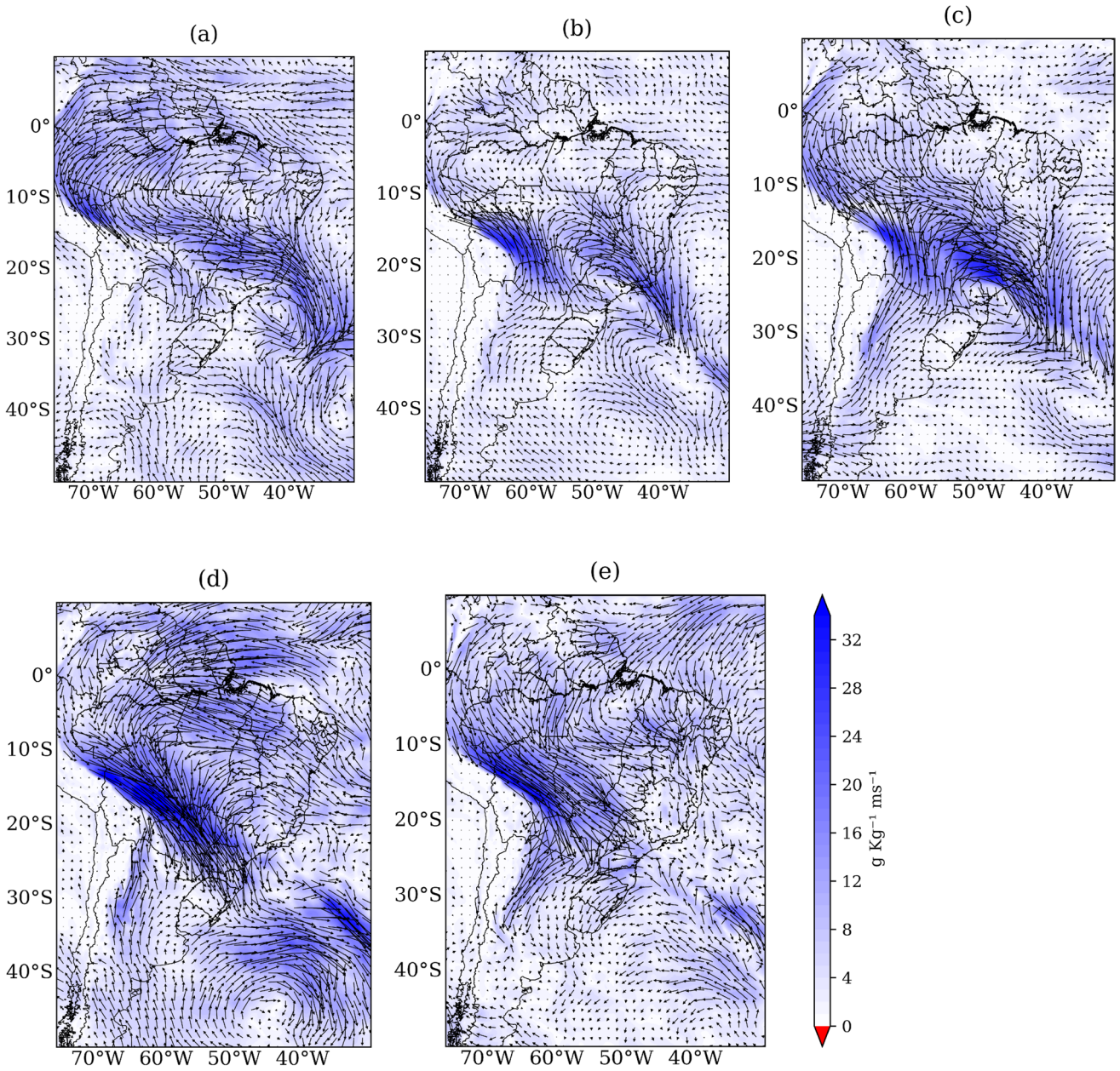

Fig. 11 Composites of moisture flux anomaly (vectors and its intensity in shaded, x10³ Kg Kg^{-1} m s^{-1}) at 850 hPa for extreme rainfall events associated with the cold fronts in MRSP for: **a** 'd-2', **b** 'd-1', **c** 'd', **d** 'd+1', **e** 'd+2'. Composites are calculated from ERA5 reanalysis for the period 1981–2022

with greater continental penetration. At the 250 hPa level, the composites for events occurring in the 'd-1' and 'd' groups showed divergence anomalies that favor upward movement. This mechanism provides a more favorable dynamic for events to occur preferentially on 'd-1' and 'd. The two event groups also exhibit cyclonic anomalies at the 850 hPa level, centered over the state of São Paulo, which also favor 'd-1' and 'd' for higher event frequency.

Especially in Fig. 11a-c, and more prominently in Fig. 11c, a well-defined cyclonic circulation is observed, centered approximately at 25°S-50°W. This type of circulation may indicate the influence of teleconnection patterns in cases of extreme rainfall events associated with cold fronts. Andrade (2017) studied the role of teleconnections in extreme rainfall events caused by frontal systems, noting that the Pacific-South American (PSA) pattern appears to influence such events during austral spring and summer. Furthermore, the anomalous circulation pattern (Fig. 11a-c) is also similar to the ones shown in Fig. 3 in Silva et al. (2021), which studied cases of SACZ associated

with cyclones in the South Atlantic. However, in the case of Silva et al. (2021), the pattern is shifted further toward the South Atlantic Ocean.

Although the present study does not search for SACZ cases, it is expected that (although unknown) some percentage of the extreme events associated with cold fronts studied here might also be associated with SACZ cases, since most of the events occur during SON and DJF. Therefore, we can also infer that the pattern in Fig. 11a-c might represent the influence of teleconnection patterns like the PSA on the SACZ, documented by Carvalho et al. (2004). According to Cavalcanti and Shimizu (2012), the PSA teleconnection pattern can influence rainfall in South America on various time scales, including the intraseasonal scale. The wave train patterns generated by the PSA can affect the amount of rainfall in SACZ events, but during austral winter, the PSA can also induce the formation and passage of cold fronts in South America (Cavalcanti and Shimizu 2012). Thus, the higher frequency of events in the 'd-1' and 'd' groups may also be influenced by the PSA teleconnection pattern.

4 Conclusions

For the period 1960–2022, in situ observations were employed to analyze the seasonality, interannual variability, trends of extreme daily precipitation events associated with cold fronts in the MRSP. Extremes are defined based on daily precipitation greater or equal to the monthly 90th percentiles. For a shorter period (1981–2022), CHIRPS data and ERA5 reanalysis were used to characterize the spatial pattern of precipitation and atmospheric circulation for extreme events associated with cold fronts. It is important to highlight that one of the limitations of the objective criterion for front identification is the use of only one station and the 10-meter wind, which is heavily influenced by local factors.

From 1960 to 2022, MRSP registered 1077 (average of 17 by year) daily precipitation extremes. There is an increase in both annual frequency and accumulated precipitation related to these extremes; moreover, both have similar interannual variability, since an increase in the number of extreme events typically results in higher cumulative rainfall.

Using a time window of 5 days (from 2 days before to 2 days after) the rainfall extremes associated with cold fronts totalized 630 events, representing a contribution of cold fronts to 58% of the daily extreme rainfall events in MRSP from 1960 to 2022, which is consistent with the approximately 50% expected for mid-latitudes of the South Hemisphere (Catto and Pfahl, 2013) and the 53% obtained by Lima et al. (2010) for southeastern Brazil.

The climatology (1960–2022) indicates that extreme rainfall associated with cold fronts preferably occurs during the austral spring (SON), although associated daily mean precipitation is higher in austral summer (the rainy season of the region). For all seasons, the extreme rainfall events associated with fronts are more frequent one day before and on the day of the detected front. From 1960 to 2022, the relative contribution of cold fronts to extreme precipitation exhibits a monotonic decreasing trend and a regime shift in 1984, which is in opposition to the increasing trend in extreme daily events in the MRSP. The discrepancy may be related to other atmospheric systems' contribution to increase in extreme events, such as isolated convection associated with urban heat island effect caused by MRSP increased urbanization (Vemado et al. 2016).

The anomalies of precipitation from CHIRPS indicate that the extremes are better characterized and occupy a larger area one day before, on the day, and one day after the cold front in MRSP. For two days before and two days after the rainfall extremes associated with cold fronts have a more local characteristic, being identified only surrounding MRSP. It is important to mention the CHIRPS underestimation of the intensity of the rainfall extremes associated with cold fronts in MRSP, which is expected since the local station represents only one point, while CHIRPS is a product combining different datasets in a horizontal grid with spacing of ~5 km.

The surface synoptic patterns of daily rainfall extremes associated with cold fronts are characterized by: (i) the presence of a surface trough over MRSP, which is connected with a surface cyclone away from the continent over the South Atlantic Ocean; (ii) a strong and well-developed post-frontal anticyclone located southwestward (northeast Argentina and south Brazil), which would sustain south quadrant winds direct to MRSP; (iii) north/northwest winds associated with the South Atlantic subtropical anticyclone/Amazon region promoting the transport of moist air to MRSP.

At mid-levels, the trough is located over south Brazil with thickness (between 500 and 1000 hPa) anomalies showing different intensity along the five days. For the 5 days window, the negative and positive thickness anomalies cover southern and southeastern Brazil, with only negative anomalies over MRSP one day before the cold front detection. Therefore, a thickness gradient (thermal gradient) is possibly an important factor for the occurrence of rainfall extremes associated with cold fronts in the region. At upper levels, the streamlines show the presence of a trough in southern South America and an anticyclonic circulation centered over the northern region of Brazil/extreme northwest of the Amazon. Except for 'd+2', the upper-level divergence anomalies cover most of center-southeastern Brazil.

The comparison of different vertical levels indicates that cold fronts associated with extreme rainfall events in MRSP present a more inclined trough between 1000 hPa and 850 hPa compared with the 500 hPa and 250 hPa levels. A strong post-frontal anticyclone and troughs at mid-upper altitudes, along with patterns of divergence and low-level

moisture availability are the main features for these events. Furthermore, most extreme events associated with cold fronts occur one day before and on the day of the cold front detection, with 209 and 173 events, respectively. Both groups exhibited more favorable dynamic conditions for the development of convective systems, such as more intense and extensive anomalies of cyclonic vorticity at low levels, cyclonic structure (centered near the state of São Paulo) in the moisture flux anomalies, and stronger divergence flow at upper levels.Additionally, the moisture flux anomaly patterns at 850 hPa indicate that the PSA teleconnection pattern may influence the higher occurrence of events in 'd-1' and 'd'.

Some of the synoptic patterns found in this study, such as a more intense thickness gradient between 500 hPa and 1000 hPa, cyclonic vorticity anomalies at lower levels, fronts with greater continental penetration, anticyclonic circulation over northern Brazil at higher levels, and a shallow trough in the mid to upper troposphere can, to some extent, be generalized to other regions of South America. These characteristics can be used to identify situations where cold fronts could potentially cause intense rainfall in other regions as well as they would be useful for future construction of statistical artificial intelligence models for predicting extreme events in MRSP.

Further studies aiming to improve the understanding of the thermodynamic profile for cases of cold fronts responsible for extreme rainfall events are relevant to better comprehending the vertical structure of these systems. Additionally, this investigation is also recommended in a future climate scenario, considering the impact of climate change as a potential intensifier of these events.

Acknowledgements The authors would like to thank the meteorological centers that provided the datasets used in this study, as well as Conselho Nacional de Desenvolvimento Científico e Tecnológico (CNPq), Fundação de Amparo à Pesquisa do Estado de São Paulo (FAPESP), Coordenação de Aperfeiçoamento de Pessoal de Nível Superior – Brasil (CAPES) and the Johannes Amos Comenius Programme (P JAC) project No. CZ.02.01.01/00/22_008/0004605, Natural and anthropogenic georisks.

Author contributions All authors contributed to the study conception and design. Material preparation and data collection were performed by C.S.S and analysis was performed by C.S.S, R.P.R. and N.M.C. The first draft of the manuscript was written by C.S.S, R.P.R and N.M.C. All authors read and approved the final manuscript.

Funding This work was supported by Conselho Nacional de Desenvolvimento Científico e Tecnológico (CNPq; Grant #305349/2022-8), Fundação de Amparo à Pesquisa do Estado de São Paulo (FAPESP; Grant #2022/05476-2), Coordenação de Aperfeiçoamento de Pessoal de Nível Superior – Brasil (CAPES; Finance Code 001), and by the Johannes Amos Comenius Programme (P JAC) project No. CZ.02.01.01/00/22_008/0004605, Natural and anthropogenic georisks.

Data availability The datasets used in this study are publicly available and can be found at: https://doi.org/10.24381/cds.6860a573 [ERA5] and https://data.chc.ucsb.edu/products/CHIRPS-2.0/ [CHIRPS]. The IAG-USP station data are available under request at http://www.estacao.iag.usp.br/sol_dados.php. The post-processed data used in this study are available at https://doi.org/10.5281/zenodo.14170016 [Zenodo].

Declarations

Competing interests The authors declare no competing interests.

References

Andrade KM (2017) O papel das teleconexões e de fatores regionais que influenciam a ocorrência de precipitação extrema associada a sistemas frontais sobre o sudeste do Brasil.Thesis, Instituto de Astronomia, Geofísica e Ciências Atmosféricas, Universidade de São Paulo

Andrade K, Cavalcanti I (2018) Atmospheric characteristics that induce extreme precipitation in frontal systems over Southeastern Brazil during summer: observations and atmospheric model simulation. Int J Climatol 38(14):5368–5385

Bonnet SM, Dereczynski CP, Nunes A (2018) Caracterização sinótica E climatológica De eventos de chuva pós-frontal no Rio De Janeiro. Revista Brasileira De Meteorologia 33:547–557

Carvalho LMV, Jones C, Liebmann B (2002) Extreme precipitation events in Southeastern South America and large-scale convective patterns in the South Atlantic Convergence Zone. J Clim 15:2377–2394

Carvalho LMV, Jones C, Liebmann B (2004) The South Atlantic Convergence Zone: intensity, form, persistence, and relationships with Intraseasonal to Interannual Activity and Extreme Rainfall. J Clim 17(1):88–108

Catto JL, Pfahl S (2013) The importance of fronts for extreme precipitation. J Geophys Res Atmos 118(19):10–791. https://doi.org/10.1002/jgrd.50852

Cavalcante RBL et al (2020) Evaluation of extreme rainfall indices from CHIRPS precipitation estimates over the Brazilian Amazonia. Atmos Res 238:104879

Cavalcanti IFA, Kousky VE (2003) Climatology of South American cold fronts International Conference on Southern Hemisphere Meteorology and Oceanography. In: Procedings… Wellington, vol 7. Amer Meteor Soc Wellington, New Zealand. p 2003

Cavalcanti IFA, Shimizu MH (2012) Climate fields over South America and variability of SACZ and PSA in HadGEM2-ES, 1:132–144. https://doi.org/10.4236/ajcc.2012.13011

Cavalcanti IF et al (2009) Tempo e Clima no Brasil. Oficina de textos, Brazil

Dalagnol R et al (2022) Extreme rainfall and its impacts in the Brazilian Minas Gerais state in January 2020: can we blame climate change? Clim Resil Sustain 1:15. https://doi.org/10.1002/cli2.15

Dametto GS, da Rocha RP (2005) Características climáticas Dos Sistemas Frontais na cidade de São Paulo. IAG/USP, São Paulo

de Jesus EM (2014) Simulações climáticas regionais para o CORDEX sobre a América do Sul e impactos das frentes frias na climatologia simulada. Dissertation, Instituto de Astronomia, Geofísica e Ciências Atmosféricas, Universidade de São Paulo

de Jesus EM, da Rocha RP, Reboita MS, Llopart M, Mosso Dutra LM, Remedio ARC (2016) Contribution of cold fronts to seasonal rainfall in simulations over the southern La Plata Basin. Clim Res 68:243–255. https://doi.org/10.3354/cr01358

de Souza DC, Crespo NM, da Silva DV et al (2024) Extreme rainfall and landslides as a response to human-induced climate change: a case study at Baixada Santista, Brazil. Nat Hazards 1–24. https://doi.org/10.1007/s11069-024-06621-1

Escobar GCJ, Seluchi ME, Andrade K (2016) Classificação Sinótica De Frentes Frias Associadas a Chuvas Extremas no Leste De Santa Catarina (SC). Revista Brasileira De Meteorologia 31(4):649–661. https://doi.org/10.1590/0102-7786312314b20150156

Escobar GCJ, Reboita M, Souza A (2019) Climatology of surface baroclinic zones in the coast of Brazil. Atmósfera 32:129–141. https://doi.org/10.20937/ATM.2019.32.02.04

Funk C et al (2015) The climate hazards infrared precipitation with stations - a new environmental record for monitoring extremes. Sci Data 2:1–21. https://doi.org/10.1038/sdata.2015.66

Garreaud R (2000) Cold air incursions over subtropical South America: Mean structure and dynamics. Mon Weather Rev 128(7):2544–2559

Haddad EA, Teixeira E (2015) Economic impacts of natural disasters in megacities: the case of floods in São Paulo. Brazil Habitat Int 45:106–113

Hersbach H et al (2020) The ERA5 global reanalysis. Q J R Meteorol Soc 146(730):1999–2049

IBGE (Instituto Brasileiro de Geografia e Estatística) (2018) Estimativas da população residente nos municípios brasileiros com data de referência 1 de julho de 2018. Available in: https://www.ibge.gov.br/estatisticas/sociais/populacao/9103-estimativas-de-populacao.html

IPCC (2014) Climate change: Synthesis report. In: Pachauri RK, Meyer LA (eds) Contribution of Working Groups I, II and III to the Fifth Assessment Report of the Intergovernmental Panel on Climate Change. IPCC, Geneva. Accessed 04.07.2024. Available online at https://www.ipcc.ch/report/ar5/syr/

IPCC (2021) Climate change: The physical science basis. In: Masson-Delmotte V, Zhai P, Pirani A, Connors SL, Péan C, Chen Y, Goldfarb L, Gomis MI, Matthews JBR, Berger S, et al. (eds) Contribution of Working Group I to the Sixth Assessment Report of the Intergovernmental Panel on Climate Change. Cambridge University Press, Cambridge. Accessed 04.07.2024. Available online: https://www.ipcc.ch/report/ar6/wg1/#FullReport

Kendall MG (1975) Rank correlation methods, 4 edn. Charles Griffin, Londres

Liebmann B, Jones C, De Carvalho LMV (2001) Interannual variability of daily extreme precipitation events in the state of Saõ Paulo. Brazil J Clim 14(2):208–218

Lima KC, Satyamurty P, Fernández JPR (2010) Large-scale atmospheric conditions associated with heavy rainfall episodes in Southeast Brazil. Theor Appl Climatol 101:121–135

Machado CB et al (2021) Extreme rainfall events in the macrometropolis of São Paulo: trends and connection with climate oscillations. J Appl Meteorol Climatology v 60(5):661–675

Magalhães SJ, Cerqueira VF, Dereczynski CP, Rehbein A, Reboita SM (2023) Cold fronts responsible for intense winds in the Santos Basin. Brazilian Southeast Offshore Region Atmósfera 37:533–550

Mann HB (1945) Non-parametric tests against trend. Econometria 13:245–259

Marengo JA et al (2020) Changing trends in Rainfall extremes in the Metropolitan Area of São Paulo: causes and impacts. Front Clim 2:3. https://doi.org/10.3389/fclim.2020.00003

Martin JE (2013) Mid-latitude atmospheric dynamics: a first course. Wiley

Montini TL, Jones C, Carvalho LMV (2019) The south American low-level jet: a new climatology, variability, and changes. J Geophys Research: Atmos 124:1200–1218

Moura CRW, Escobar GCJ, Andrade KM (2013) Padrões De circulação em superfície e altitude associados a eventos de chuva intensa na Região Metropolitana do Rio De Janeiro. Rev bras Meteorol 28(3):267–280. https://doi.org/10.1590/S0102-77862013000300004

Nieto-Ferreira R, Rickenbach TM, Wright EA (2011) The role of cold fronts in the onset of the monsoon season in the South Atlantic convergence zone. Q J R Meteorol Soc 137:908–922. https://doi.org/10.1002/qj.810

Paiva DA, Sáfadi T (2021) Study of tests for trend in time series. Brazilian J Biometrics 39:2

Pampuch LA, Ambrizzi T (2015) Sistemas Frontais Sobre a América do Sul Parte II: Climatologia E intervalo de passagem em dados de Reanálise I do Ncep/Ncar. In:IX workshop Brasileiro De Micrometeorologia. Santa Maria-RS, Brasil

Perez GMP, Silva Dias MAF (2017) Long-term study of the occurrence and time of passage of sea breeze in São Paulo, 1960–2009. Int J Climatol 37:1210–1220

Pettitt AN (1979) A Non-parametric Approach to the Change-Point Problem. J Royal Stat Soc Ser C (Applied Statistics) 28:126–135. https://doi.org/10.2307/2346729

Pohlert T (2016) Non-parametric trend tests and change-point detection. CC BY-ND 4

Reboita MS, Gan MA, da Rocha RP, Ambrizzi T (2010) Regimes de precipitação na América do sul: uma revisão bibliográfica. Rev Bras Meteorol 25(2):185–204. https://doi.org/10.1590/S0102-77862010000200004

Reboita M, Machado Crespo N, Gozzo LF (2023) Uma introdução à análise de massas de ar, frentes e ciclones extratropicais na América do sul. Revista Brasileira De Geografia Física 16:6

Rodrigues ML, Sugahara FD S (2004) Climatologia De frentes frias no litoral de Santa Catarina. Revista Brasileira De Geofísica 22:135–151. https://doi.org/10.1590/S0102-261X2004000200004

Rodriguez CAM, Da Rocha RP, Bombardi R (2010) On the development of summer thunderstorms in the city of São Paulo: Mean meteorological characteristics and pollution effect. Atmos Res 96:477–488

Segura CS, da Rocha RP (2024) Tendências E variabilidade climática de frentes frias e precipitação na região metropolitana de São Paulo. Revista Brasileira De Climatologia 34:159–179. https://doi.org/10.55761/abclima.v34i20.17145

Seluchi M, Beu C, Andrade K (2016) Características das frentes frias com potencial para provocar chuvas intensas na região serrana do Rio De Janeiro. Rev Bras Climatologia 18. https://doi.org/10.5380/abclima.v18i0.45369

Seluchi M, Beu C, Andrade K (2017) Características das Frentes Frias Causadoras De Chuvas Intensas no Leste De Santa Catarina. Revista Brasileira De Meteorologia 32:25–37. https://doi.org/10.1590/0102-778632120150095

Silva JPR, Reboita MS, Escobar GCJ (2021) Caracterização da Zona de Convergência do Atlântico Sul em campos atmosféricos recentes. Revista Brasileira De Climatologia, *25*. https://doi.org/10.5380/abclima.v25i0.64101

Silva Dias MAF et al (2013) Changes in extreme daily rainfall for São Paulo, Brazil. Clim Change 116:705–722

Solari FI, Blazquez J, Solman S (2022) Relationship between frontal systems and extreme precipitation over southern South America. Int J Climatol 42. https://doi.org/10.1002/joc.7663

Sugahara S, Rocha R, Silveira R (2009) Non-stationary frequency analysis of extreme daily rainfall in Sao Paulo, Brazil. Int J Climatol 29:1339–1349

Vemado V, Pereira Filho AJ (2016) Severe weather caused by heat island and sea breeze effects in the Metropolitan Area of São Paulo, Brazil. Adv Meteorol 2016:ID83641341–ID836413414